Strain dependence of the nonlinear optical properties of strained Si nanoparticles

Soumen Dhara,[1,*] Kenji Imakita,[1] P. K. Giri,[2] and Minoru Fujii[1,3]

[1]*Department of Electrical and Electronic Engineering, Graduate School of Engineering, Kobe University, 1-1 Rokkodai, Nada, Kobe 657-8501, Japan*

[2]*Department of Physics, Indian Institute of Technology Guwahati, Guwahati 781 039, India*

[3]*e-mail: fujii@eedept.kobe-u.ac.jp*

**Corresponding author: soumen5484@yahoo.co.in*

Received April 22, 2014; revised May 26, 2014; accepted May 26, 2014;
posted May 27, 2014 (Doc. ID 210330); published June 23, 2014

We report on the lattice strain dependence of the nonlinear optical (NLO) parameters of strained Si nanoparticles (NPs), which are prepared in a controlled way by a mechanical ball milling process. X-ray diffraction analysis shows that the nature of strain is compressive and is primarily caused by milling-induced lattice dislocations, which is further supported by high-resolution transmission electron microscopy imaging. It is found that the nonlinear refractive index (n_2) and nonlinear absorption coefficient (β) are strongly influenced by the associated lattice strain present in Si NPs. With the increase of lattice strain, the β gradually decreases while n_2 increases slowly. The strain-dependent observed changes in the NLO parameters of Si NPs are found to be advantageous for application purpose, and it is explained on the basis of strain-induced modification in the electronic structure of the highest occupied molecular orbital and lowest unoccupied molecular orbital states of Si NPs. These results demonstrate the potential of strain-dependent enhancement of nonlinearities for silicon photonics applications. © 2014 Optical Society of America

OCIS codes: (160.4330) Nonlinear optical materials; (190.4720) Optical nonlinearities of condensed matter.
http://dx.doi.org/10.1364/OL.39.003833

Nanomaterials, having excellent nonlinear optical (NLO) properties, exhibit considerable promise for the use in optical switch and transmission of high bit rate multiple optical signals. Si is a well-known narrow-bandgap semiconductor, and its nanostructures are promising candidates for such applications. Recently, nonlinear Si devices have been demonstrated for a wide range of applications [1–3]. NLO properties of Si nanocrystals (NCs) embedded in a matrix (mainly silica) are extensively studied, β and n_2 are found to be strongly dependent on the fabrication process [4–6]. None of the previous studies considered the effects of external strain caused by silica matrix or even internal lattice strain on the obtained NLO response from the Si NCs. Furthermore, technologically it is almost impossible to prepare fine Si NCs without any strain. Several previous studies on Si NCs pointed out that strain has a strong influence on the linear optical properties of Si, and it can be tailored through effective strain engineering [7–11]. Thean and Leburton studied the strain effect in large Si NCs (10 nm) embedded in SiO_2 and showed that coupling between Si NCs and the strain potential can enhance the confinement [7]. Axial-stress-dependent bandgap tuning by strain-field-induced band splitting is also elucidated in Si nanowires [12]. In a recent theoretical study, Jiang *et al.* [11] showed that uniaxial compression on the Si nanoparticles (NPs) redistributes the isosurface of the highest occupied molecular orbital (HOMO) and lowest unoccupied molecular orbital (LUMO) wave functions along the strain orientation, and, hence, a strong influence on the optical absorption spectra could be seen. Therefore it is important to distinguish any effect of strain on the NLO parameters of Si NCs. In our previous study, we prepared freestanding Si NPs with sizes 43–10 nm by the mechanical ball milling process for a time duration of 2–30 h and studied their size-dependent visible absorption and photoluminescence [13]. Furthermore, these Si NPs are strained and contain lattice strain varying from 0.21% to 0.53%. These samples enable us to investigate only the strain dependence on the NLO response of Si NPs.

In this Letter, we report the influence of lattice strain on the NLO properties of strained Si NPs. The third-order nonlinearity of the freestanding Si NPs is measured by the standard Z-scan technique after embedding in a poly(methyl methacrylate) (PMMA) film. This study is performed in the size regime of Si NPs above the excitons-Bhor radius. Therefore, no contribution from quantum size effect is expected. We proposed that strain-induced modification in the electronic structure of HOMO and LUMO states of Si NPs is probably responsible for the observed strain-dependent behavior.

Freestanding Si NPs were prepared from commercially available high-purity Si powder (average particle size ~75 μm, Sigma Aldrich) using the mechanical ball milling method. Ball milling was performed at 450 rpm for a duration up to 30 h in a zirconium oxide vial (Restch, PM100) under atmospheric condition using small zirconium oxide balls. Very fine Si NPs with few nanometer sizes were obtained after 2, 5, 10, 20, and 30 h of milling and used for this study. These samples are named Si-2, Si-5, Si-10, Si-20, and Si-30, respectively, along with the starting Si powder as Si-0. The powder samples were analyzed by powder x-ray diffraction (XRD, Seifert 3003T/T) for the determination of crystal quality, average NPs size, internal lattice strain, and dislocation density. Evolution of strain with decrease in size of the NPs is analyzed from the extensive analysis of the XRD line profile and further confirmed from the high-resolution transmission electron microscopy (TEM) (JEOL, JEM 2100F) studies, according to the method as discussed in detail in our previous reports [9,13].

For the measurement of NLO properties, above-prepared freestanding Si NPs were embedded inside the PMMA matrix. First a transparent solution of PMMA

 © 2014 Optical Society of America

in chloroform (100 gm/L) was prepared, and then Si NPs were slowly added during stirring followed by sonication for 1 h. The weight concentration of Si NPs in PMMA was maintained at 0.5% for all the samples. Next, the above-prepared solution mixtures were spin-coated on quartz substrates followed by a hot air dry at 60°C for 1 h. In this process, we prepared highly transparent PMMA thin films containing Si NPs with a thickness of about 2 μm. The Z-scan technique [14] measurement was performed by translating the sample through a tightly focused Gaussian beam along the direction of the beam propagation (z axis) and measuring the transmitted power. We used a linearly polarized femtosecond pulse beam (at 800 nm) from a mode-locked Ti:sapphire laser (Tsunami) with a pulse width of 70 fs and repetition frequency of 82 MHz. An aperture was placed in front of the detector during transmitted power measurement. A completely open aperture (OA) without obstructing any incoming light indicates the OA condition; a partially closed aperture (CA) with some fraction of transmitted light to the detector refers to the CA condition. The incident peak intensity was maintained at 12.5 GW/cm^2.

Due to high-speed grinding, a significant reduction in particle size is observed after 2–30 h of milling. A 30 h milled sample contains NPs with log-normal-type size distribution from 8–14 nm. The as-prepared Si NPs are highly crystalline as indicated by XRD patterns and high-resolution lattice fringe images. During the milling process, owing to deformation, strain is expected in as-prepared Si NPs. The XRD patterns for different samples are used for the calculations of lattice strain by the Williamson–Hall (WH) method [15] and average NPs size and dislocation density by the Ungar–Borbely method [16]. It is found that the nature of the strain is compressive and is primarily caused by milling-induced lattice dislocations. Figure 1 shows the evolution of lattice strain and dislocation density of the Si NPs with the increase of milling time. The inset shows the XRD pattern (Si-10) and NPs size as a function of milling time. This analysis shows that the average NP size monotonically goes down from 43 to 10 nm as the milling time increases from 2 to 30 h. On the other hand, the lattice strain/dislocation density first increases up to 10 h of milling and then slowly decreases for higher milling time. This can be explained as follows: during milling, the strain and dislocations first develop; however, for prolonged milling when the dislocation density is high, the crystal breaks up along the slip plane and thus produces smaller sized NCs. In this way, strain is partly released for a prolonged milling time. We further verified the associated lattice strain after embedding the Si NPs inside the PMMA, and the change of lattice strain is negligible in this case.

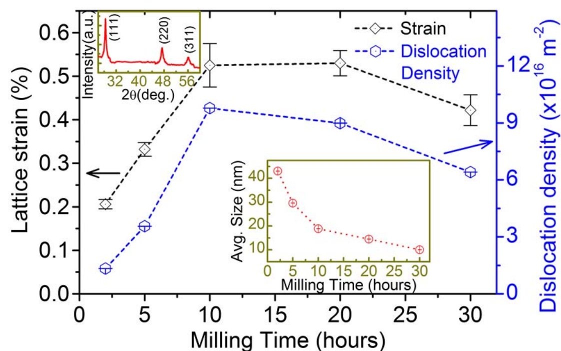

Fig. 1. Evolution of lattice strain and dislocation density with the milling time for Si NPs. Inset (top): XRD pattern of Si-10 NPs. Inset (bottom) graph shows the reduction of Si NPs size with milling time.

Figure 2(a) shows the high-resolution TEM image of lattice fringes of single as-prepared Si-10 NPs, which clearly shows the existence of several lattice dislocations (regions marked with rectangles). Gradual accumulation of this dislocation in the Si lattice results in shrinkage of lattice spacing. Careful analysis shows that the interplanar spacing $d_{\langle 111 \rangle}$ decreases from 3.13 to 2.95 Å because of size reduction, implying that a compressive strain developed during milling. Therefore a high-resolution TEM image provides clear evidence of lattice dislocations, which induced compressive strain in the Si NPs. In order to release some strain, the above Si-10 NPs are subjected to annealing at 500°C for 1 h in Ar medium. Before the purging of Ar gas, the sample chamber was evacuated to the high vacuum of $\sim 10^{-4}$ mbar. A high-resolution lattice fringe image [Fig. 2(b)] of the annealed Si-10 NPs shows better crystalline structure with significant reduction of lattice dislocations. Furthermore, lattice spacing increased to 3.11 Å, which indicates noticeable strain relaxation during thermal annealing. During annealing, the system undergoes a partial recrystallization process, and release of associated lattice strain is expected.

The linear absorption spectra [Fig. 3(a)] of the strained Si NPs in PMMA thin films show a highly transparent nature from the visible to NIR range, and a very small fraction of incident light is absorbed. However, it shows a strong absorption below 400 nm from all the samples, and it arises from the interband transition of Si NPs [17]. The milled Si NPs exhibit enhanced absorption in the red-orange region of the visible spectrum. Furthermore, this absorption band shows gradual blueshifting with an increase of milling time. It is considered that strain-induced modification in the electronic band structure of the Si NPs and its influence on the quasi-direct-like transition is mainly responsible for the observed visible absorption band. A detailed discussion about similar results of visible absorption of Si NPs could be found in our previous report [9].

Figures 3(b) and 3(c) show the typical Z-scan measurement data for the Si-10 sample. We observed a dip in the

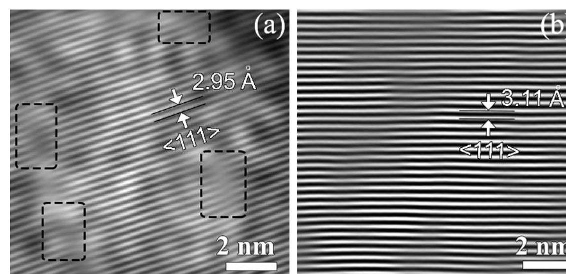

Fig. 2. (a) HRTEM lattice image of Si-10 nanoparticle showing distorted and shrunk lattice (regions marked with rectangle) due to the presence of compressive lattice strain. (b) HRTEM lattice image of Si-10 after annealing showing improvement in the lattice distortion by release of strain.

OA condition and a valley-to-peak in the CA condition in transmittance curves. Measurement on pure PMMA thin film shows no significant NLO contribution; thus the influence of the PMMA matrix on the present Z-scan data may be considered negligible. As the OA data is directly related to the nonlinear absorption coefficient, the observed dip indicates the reverse saturation absorption, and β is positive. The valley-to-peak behavior in the CA condition further indicates the self-focusing and mainly refractive-type nature, and the corresponding n_2 is positive. To evaluate the NLO contribution and in order to quantify the NLO parameters, we fitted the experimental transmittance data with the following expressions [4,14]:

In OA configuration,

$$T^{\mathrm{OA}}(z) = 1 - \frac{\beta I_0 L}{1 + \left(\frac{z}{z_0}\right)^2}, \tag{1}$$

for the ratio of transmittance in CA and OA configurations,

$$\frac{T^{\mathrm{CA}}(z)}{T^{\mathrm{OA}}(z)} = 1 + \frac{4\Delta\varphi\left(\frac{z}{z_0}\right)}{\left[1 + \left(\frac{z}{z_0}\right)^2\right]\left[9 + \left(\frac{z}{z_0}\right)^2\right]}, \tag{2}$$

where I_0, L, z_0, and $\Delta\varphi$ represent the peak intensity of the laser beam, sample thickness, Rayleigh diffraction length of the beam (~1.1 mm in the present laser beam), and nonlinear phase change, respectively. Finally, the nonlinear refractive index, n_2, is determined from $\Delta\varphi$ by

$$n_2 = \frac{\lambda \alpha \Delta\varphi}{2\pi I_0 (1 - e^{-\alpha L})}, \tag{3}$$

where α is the linear absorption at the used wavelength λ. The estimated values of β and n_2 are of the order of $\sim 10^{-8}$ cm/W and $\sim 10^{-12}$ $\mathrm{cm^2/W}$, respectively. Here we note that the obtained value of n_2 is two orders of magnitude larger than the bulk Si [4]. The nonlinear figure of merit (NFOM) for the optical switching applications obtained by $n_2/\beta\lambda$ is as high as 1.83 for the Si-10, which is much larger than the case of bulk Si (~0.4) [18] and also two times larger than the starting Si powder (0.89).

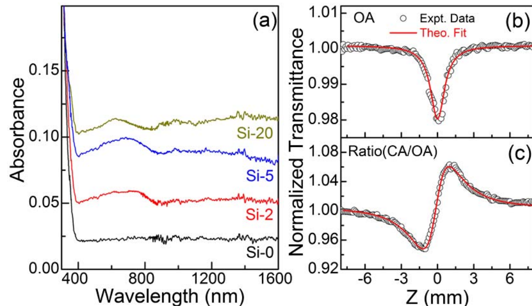

Fig. 3. (a) Linear absorption spectra of Si NPs with different sizes and strain. Z-scan measurement data in (b) open aperture (OA) and (c) ratio of closed aperture (CA) to OA configurations for the Si NPs (Si-10). The solid lines are theoretical fitting using Eqs. (1) and (2), respectively.

The variation of β and n_2 are plotted in Figs. 4(a) and 4(b) as a function of the lattice strain present in the Si NPs. The n_2 and β are strongly influenced by the associated lattice strain and show nonmonotonic enhancement with the accumulation of strain. It is found that the β first increases with the incorporation of strain and then decreases with further accumulation of strain up to 0.52%. With further increase of strain, it starts to increase. In this process, β decreases from 1.4×10^{-8} cm/W to 1.0×10^{-8} cm/W. On the other hand, n_2 slowly increases from 0.99×10^{-12} $\mathrm{cm^2/W}$ to 1.45×10^{-12} $\mathrm{cm^2/W}$ up to 0.52% of strain accumulation and then suddenly decreases with further increase of strain. Here we assumed that the starting Si powder/particles are almost strain free due to the limitation of the strain estimation by the WH method for this sample (the WH method is applicable to the particles with sizes below 1 μ). We believe that a significant modification in the electronic band structure of Si NPs caused by the associated compressive strain may be responsible for the observed improvement in the NLO response. Lattice under compression undergoes a structural deformation by reduction of cluster symmetry and changes in bond angle and bond length. Such strain-induced deformation may lead to modification of HOMO and LUMO wave functions and, hence, resultant linear and NLO properties. Here we observed a visible absorption band after accumulation of compressive lattice strain. Recent theoretical studies show that electronic and optical properties of Si NPs are significantly modified by the associated lattice strain [10,11,19]. One study pointed out that redistribution of HOMO and LUMO wave functions along the strain direction is mainly responsible for the observed changes, while another study pointed out that, inside the Si band diagram, electronic charge densities of various energy states vary with strain, and they have different dependence. The sudden increase of β and decrease of n_2 for the Si-20 at a lattice strain of 0.53% may be due to the additional influence by defects. Two types of defects are present in these Si NPs: dislocation defects and interface defects. Both defects have some positive impact on the magnitude of n_2 and β. It is also known that the dependence of β on the interface defect is stronger than n_2. Between the samples Si-10 and Si-20, the increase of strain is less (0.01%),

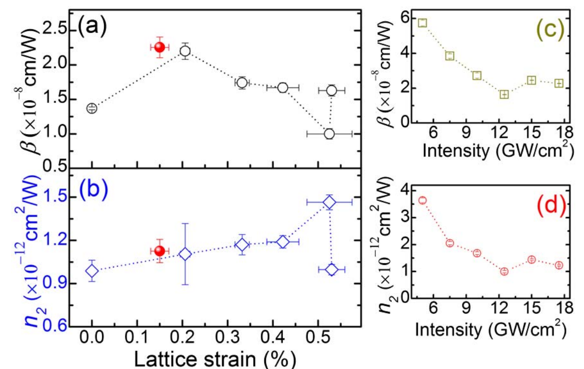

Fig. 4. Lattice strain dependence of (a) β and (b) n_2 for the Si NPs measured at a peak power of 12.5 $\mathrm{GW/cm^2}$. Red color data points are for the Si-10 after thermal annealing. (c) and (d) Nonlinear parameters β and n_2 as a function of incident peak laser power for the Si NPs (Si-20).

and there is a decrement of dislocation defects density (8.1%). Along with them, a huge enhancement of interface defects is expected with an additional 10 h of milling. Then the collective dependence of strain, dislocation defects, and interface defects results in a sudden increase of β and decrease of n_2 for Si-20. Since the quantum confinement is unlikely to play any role in this size regime of Si NPs, the observed changes in the n_2 and β are believed to be mainly lattice strain dependent behavior. Previous studies reported significant enhancement of NLO parameters for small Si NCs, about 2–5 nm, embedded in SiO_2 [4,20,21]. The observed enhancement is explained on the basis of a dimensional confinement induced transition in the Si NCs. Previous studies further pointed out that defects can also enhance the NLO response of Si NCs and, hence, the n_2 and β [22]. However, in the present case, the changes of n_2 and β follow an opposite trend, which rules out the dependence of only defects in the observed changes. Therefore, associated compressive strain is mainly responsible for the observed changes in the NLO response of Si NPs. To confirm further, the NLO response of annealed Si-10 NPs is measured by the same process, and the estimated values of n_2 and β are shown in Figs. 4(a) and 4(b) (red data points). Thermal annealing of Si-10 caused significant reduction of strain from 0.52% to 0.15%, which is consistent with the observed high-resolution TEM image. Interestingly, the magnitude of n_2 and β of annealed Si-10 resides close to the projected line of the strain-dependent behavior of n_2 and β. Therefore it is further confirmed that there is strong dependence of NLO properties of Si NPs on the associated compressive lattice strain. The observed enhancement of n_2 and decrement of β with the evolution of lattice strain is advantageous for photonics applications. Therefore incorporation of small amounts of lattice strain in the Si NPs is found to be advantageous.

To verify further, we measured the incident power dependence on the NLO parameters for the Si-20 sample [Figs. 4(c) and 4(d)]. Initially at lower power, both the NLO parameters show comparatively high values ($n_2 \sim 3.64 \times 10^{-12}$ cm^2/W and $\beta \sim 5.74 \times 10^{-8}$ cm/W) and then gradually decrease with the increase of incident power and stabilize at higher power. Other samples show similar dependence of n_2 and β on the incident power. Observed power dependence of n_2 and β is similar to the previously reported NLO response of Si rich silicon oxide film [23]. This behavior can be explained by considering the contributions from bound electrons and excited carriers by two photon absorption on the NLO response. At low peak intensities, contribution from the bound electronic effect dominates over the contribution due to excited carriers, whereas, with increase of peak intensities, the negative contribution from excited carriers increases, resulting in decrease of NLO response. The stabilization of n_2 and β at higher pump power may be due to the saturation in the excited carriers population induced band-filling effect.

We investigated the lattice strain dependence of the NLO response of strained Si NPs by Z-scan technique. Si NPs with a different percentage of lattice strain are prepared. XRD analysis shows that the nature of strain is compressive, and it is primarily caused by milling-induced lattice dislocations, which is further supported by TEM imaging. It is found that n_2 and β are strongly influenced by the associated lattice strain present in the Si NPs. With the increase of lattice strain, the β gradually decreases while n_2 increases slowly, which is found to be advantageous for photonics application purposes. These results demonstrate the potential of strain-dependent enhancement of nonlinearities in Si NPs and the possibility of effective strain engineering.

Part of the experiment was carried out under Grant-in-Aid for Scientific Research (KAKENHI 24-02316) from the Japan Society for the Promotion of Science (JSPS). S. D. acknowledges the postdoctoral fellowship from JSPS.

References

1. A. M. Armani, R. P. Kulkarni, S. E. Fraser, R. C. Flagan, and K. J. Vahala, Science **317**, 783 (2007).
2. J. Leuthold, C. Koos, and W. Freude, Nat. Photonics **4**, 535 (2010).
3. P. Koonath, D. R. Solli, and B. Jalali, Appl. Phys. Lett. **91**, 061111 (2007).
4. K. Imakita, M. Ito, M. Fujii, and S. Hayashi, J. Appl. Phys. **105**, 093531 (2009).
5. S. Minissale, S. Yerci, and L. D. Negro, Appl. Phys. Lett. **100**, 021109 (2012).
6. S. Lettieri and P. Maddalena, J. Appl. Phys. **91**, 5564 (2002).
7. A. Thean and J. P. Leburton, Appl. Phys. Lett. **79**, 1030 (2001).
8. X.-H. Peng, S. Ganti, A. Alizadeh, P. Sharma, S. K. Kumar, and S. K. Nayak, Phys. Rev. B **74**, 035339 (2006).
9. S. Dhara and P. K. Giri, Nanoscale Res. Lett. **6**, 320 (2011).
10. C. Zhang, A. D. Sarkar, and R.-Q. Zhang, J. Phys. Chem. C **115**, 23682 (2011).
11. X. Jiang, J. Zhao, and X. Jiang, J. Nanopart. Res. **14**, 818 (2012).
12. A. J. Lu, R. Q. Zhang, and S. T. Lee, Appl. Phys. Lett. **91**, 263107 (2007).
13. S. Dhara and P. K. Giri, J. Nanosci. Nanotechnol. **11**, 9215 (2011).
14. M. Sheik-Bahae, A. A. Said, T. H. Wei, D. J. Hagan, and E. W. V. Stryland, IEEE J. Quantum Electron. **26**, 760 (1990).
15. G. K. Williamson and W. H. Hall, Acta Metall. **1**, 22 (1953).
16. T. Ungar and A. Borbely, Appl. Phys. Lett. **69**, 3173 (1996).
17. E. L. d. Oliveira, E. L. Albuquerque, J. S. d. Sousa, and G. A. Farias, Appl. Phys. Lett. **94**, 103114 (2009).
18. A. D. Bristow, N. Rotenberg, and H. M. v. Driel, Appl. Phys. Lett. **90**, 191104 (2007).
19. C. S. Lin, W. D. Cheng, J. Y. Wang, and R. Q. Zhang, Chem. Phys. Lett. **509**, 124 (2011).
20. Anchala, S. P. Purohit, and K. C. Mathur, J. Appl. Phys. **110**, 114320 (2011).
21. G. V. Prakash, M. Cazzaneli, Z. Gaburro, L. Pavesi, F. Lacona, G. Franzo, and F. Priolo, J. Appl. Phys. **91**, 4607 (2002).
22. M. Ito, K. Imakita, M. Fujii, and S. Hayashi, J. Appl. Phys. **108**, 063512 (2010).
23. R. Spano, N. Daldosso, M. Cazzanelli, L. Ferraioli, L. Tartara, J. Yu, V. Degiorgio, E. Jordana, J. M. Fedeli, and L. Pavesi, Opt. Express **17**, 3941 (2009).